Tunneling of Dirac electrons through spatial regions of finite mass

2008 J. Phys.: Condens. Matter 20 325221

(http://iopscience.iop.org/0953-8984/20/32/325221)

J. Phys.: Condens. Matter **20** (2008) 325221 (12pp) doi:10.1088/0953-8984/20/32/325221

Tunneling of Dirac electrons through spatial regions of finite mass

J Viana Gomes and N M R Peres

Center of Physics and Department of Physics, University of Minho, P-4710-057, Braga, Portugal

Received 25 March 2008, in final form 14 May 2008
Published 9 July 2008
Online at stacks.iop.org/JPhysCM/20/325221

Abstract

We study the tunneling of chiral electrons in graphene through a region where the electronic spectrum changes from the usual linear dispersion to a hyperbolic dispersion, due to the presence of a gap. It is shown that, contrary to the tunneling through a potential barrier, the transmission of electrons is, in this case, smaller than one for normal incidence. This mechanism may be useful for designing electronic devices made of graphene.

(Some figures in this article are in colour only in the electronic version)

1. Introduction

A new and exciting field in condensed matter physics started when graphene—a two-dimensional, one carbon-atom thick material—was isolated for the first time [1, 2]. It was experimentally shown that the charge carriers in graphene could be controlled by a bottom gate set-up; the charge carrier were shown to be either holes or electrons, depending on the sign of the bottom gate voltage. In the transition from hole-based to electron-based transport the conductivity shows a minimum (not zero) value, $\sigma_{\min}$. Its experimental value is of the order of $\sigma_{\min} \simeq 4e^2/h$ [1–4], but the actual value seems to be somewhat sample-dependent [5]. This value for $\sigma_{\min}$ imposes therefore a limitation on the minimum value of the current a field effect transistor made of graphene can transport. The existence of a conductivity minimum in graphene is a consequence of the fact that the elementary excitations of graphene are Dirac fermions, with a linear dispersion relation, instead of the usual electrons with parabolic-like dispersion, characteristic of ordinary semiconductors. Interestingly enough, the calculated value of the conductivity of graphene at the neutrality point is off the experimental value by the factor $1/\pi$ [6–8]. Although this value is the more common result for the theoretical calculation of $\sigma_{\min}^{\text{theo}}$, there are, however, several different values available in the literature [9]. It is also interesting that a clean graphene sample with metallic leads and smooth edges has a value of $\sigma = \sigma_{\min}^{\text{theo}}$ as long as its width (w) is much larger than its length (L), being smaller than $\sigma_{\min}^{\text{theo}}$ in the opposite limit [10]. Considering the case of metallic armchair edges, it found that $\sigma > \sigma_{\min}^{\text{theo}}$ for $w/L \ll 1$ and that $\sigma \to \sigma_{\min}^{\text{theo}}$ for $w/L \gg 1$ [10]. This shows that disorder is not needed for having $\sigma \simeq \sigma_{\min}^{\text{theo}}$.

Another characteristic of Dirac electrons in graphene is their ability to tunnel through a potential barrier with probability one [11, 12]. This so-called Klein tunneling of chiral particles has long ago been proposed in the framework of quantum electrodynamics [13–15], but was never observed experimentally. Graphene opens up a route to observe this effect in a tabletop experiment, where the potential is created by some electrostatic gate potential. The manifestation of Klein tunneling is also present when electrons in graphene are forced to transverse an n–p junction, leading to a selective transmission of those electrons approaching the junction perpendicularly [16]. Other unusual effects, such as the focusing of an electric current by a single p–n junction, are also characteristic of Dirac electrons in graphene [17].

As appealing as the Klein tunneling may sound from the point of view of fundamental research, its presence in graphene is unwanted when it comes to applications of graphene to nanoelectronics. This comes about because the pinch-off of the field effect transistor may be very ineffective. The same may occur because of the minimum conductivity of graphene at the neutrality point (as discussed above). One way to overcome these difficulties is by generating a gap in the spectrum. From the point of view of Dirac fermions this is equivalent to the generation of a mass term. There are two known forms of generating gaps in the spectrum of graphene. The first one is by patterning graphene nanoribbons [18, 19]. The mechanism of producing these gaps depends on the nature of the termination of these nanoribbons. For armchair nanoribbons the gap comes from quantum confinement of Dirac fermions induced by the finite nature of the ribbons in the transverse direction. For zigzag nanoribbons the gap stems from the formation

of polarized spin edge states characteristic of these type of ribbons. The formation of these polarized states is also possible in bilayer graphene [20]. It is interesting to notice that Klein tunneling can also be circumvented by using a graphene bilayer [11]. The value of the induced gaps depends on the width of the ribbons, but for large widths it is of the order of 0.1 eV.

Another possibility of generating gaps in the graphene spectrum is to deposit graphene on top of hexagonal boron nitride (BN) [21]. This material is a bandgap insulator with a boron to nitrogen distance of the order of 1.45 Å [23] (in graphene the carbon–carbon distance is 1.42 Å) and a gap of the order of 4 eV. It was shown that, in the most stable configuration, where a carbon is on top of a boron and the other carbon in the unit cell is centered above a BN ring, the value of the induced gap is of the order of 53 meV. Depositing graphene on a metal surface with a BN buffer layer leads to n-doped graphene with an energy gap of 0.5 eV [22].

The two mechanisms described above can be used to produce arrangements of graphene where in some spatial zones of the material the Dirac electrons will have gaps in the spectrum. The first possibility is to pattern graphene planes such that, in several areas of the graphene flake, narrow nanoribbons may exist. Another possibility is to combine wafers of silicon oxide and hexagonal boron nitride, such that in the region where the BN is located the local spectrum of graphene will present a finite gap. We shall explore in this paper this latter possibility and the way it can prevent Klein tunneling from occurring. The two mechanisms just mentioned can then be at the heart of future nanoelectronics built of graphene. The second method is also related to junctions of graphene with other kinds of systems, being then superconducting [24, 25], normal-conductor/graphene/normal-conductor [26] or multiterminal junctions [27]. Also the study of electron transport in disordered graphene samples is of interest [28], especially because the tunneling may be assisted by impurities [29], which is a manifestation of Klein tunneling.

For a review of the experimental aspects of graphene physics see the work of Geim and Novoselov [30]. Some of the theoretical aspects of graphene physics are reviewed qualitatively by Castro Neto *et al* [31], Katsnelson [32] and Geim and MacDonald [33]; a more comprehensive review is given by Castro Neto *et al* [34]. For a review on Klein tunneling see the work by Beenakker [35].

2. Basic definitions

As described in the previous section, we assume that it is possible to manufacture slabs with SiO_2–BN interfaces, on top of which a graphene flake is deposited. This will induce spatial regions where graphene has a vanishing gap intercalated with regions where the BN will cause a finite gap.

In the following we will consider the graphene physics in two different regions: the k-region, where the graphene sheet is standing on top of SiO_2, and a q-region, where a mass-like term is present, caused by BN, inducing an energy gap of value $2t'$ (for all numerical purposes we use $t' = 0.1$ eV). The wavefunctions in these two regions will be referred to by $\psi_{\mathbf{k}}$ and $\psi_{\mathbf{q}}$, respectively. The geometry of the scattering process is represented in figure 1.

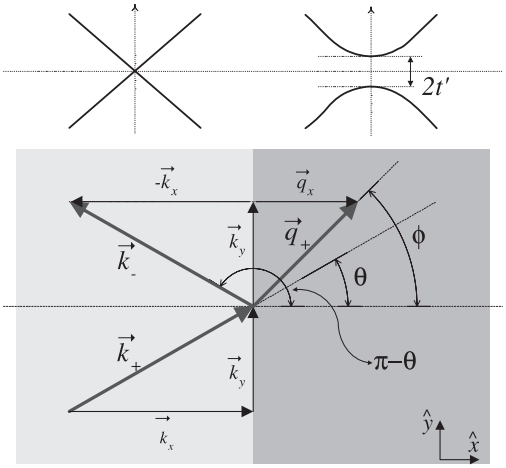

Figure 1. Top figure: graphene band structure for the massless and massive cases. In the latter, the quasi-parabolic bands have a gap energy $2t'$. Bottom figure: geometry in the reflection in the k–q interface. An incident wavefunction ψ_k^+ with wavevector $\mathbf{k}_+$ is reflected and refracted into the ψ_k^- and the ψ_q^+ wavefunctions with wavevectors $\mathbf{k}_-$ and $\mathbf{q}_+$, respectively. Since the momentum is conserved at the interface, one has that $\mathbf{q}_y = \mathbf{k}_y$. The refracted wave propagates with an angle ϕ, which is slightly larger than the incident and reflected angles θ with $|\mathbf{q}_x| < |\mathbf{k}_x|$, a consequence of energy conservation.

The Hamiltonian for massless Dirac electrons in graphene, around the $\boldsymbol{K}$-point in the Brillouin zone, is given by

$$H_g = v_F \boldsymbol{\sigma} \cdot \boldsymbol{p}, \tag{1}$$

where $\boldsymbol{\sigma} = (\sigma_x, \sigma_y)$, $\boldsymbol{p} = -\mathrm{i}\hbar\nabla$, σ_i, with $i = x, y, z$, is the i Pauli matrix, and $v_F = 3ta/(2\hbar)$, with t the nearest-neighbor hopping matrix in graphene and a the carbon–carbon distance. Therefore, in the massless wavefunction, in the k-region ($t' = 0$), it is given by

$$\psi_{\mathbf{k},s} = \frac{1}{\sqrt{2}} \begin{pmatrix} 1 \\ u(\mathbf{k}, s) \end{pmatrix} \mathrm{e}^{\mathrm{i}\mathbf{k}\cdot\mathbf{r}}, \tag{2}$$

with

$$u(\mathbf{k}, s) = s\, \mathrm{e}^{\mathrm{i}\theta}, \tag{3}$$

$s = \mathtt{sign}(E)$ and $\theta = \arctan(k_y/k_x)$. The corresponding energy eigenvalue is

$$E = \pm v_F \hbar \sqrt{k_x^2 + k_y^2} = \pm \hbar v_F k, \tag{4}$$

with k the absolute value of the wavevector.

In a region of finite mass the Hamiltonian for Dirac electrons is

$$H_g = v_F \boldsymbol{\sigma} \cdot \boldsymbol{p} + t' \sigma_z, \tag{5}$$

with $m v_F^2 = t'$ the mass term (m is the effective mass); as a consequence the electronic spectrum will present a finite energy gap of value $2t'$. In the q-region (the gapped region, $t' \neq 0$), the wavefunction is

$$\psi_{\mathbf{q},s} = \frac{1}{\sqrt{2}} \begin{pmatrix} 1 \\ v(\mathbf{q}, s)\, \mathrm{e}^{\mathrm{i}\mathbf{q}\cdot\mathbf{r}} \end{pmatrix}, \tag{6}$$

where

$$v(\mathbf{q}, s) = \frac{E - t'}{\hbar v_F (q_x - \mathrm{i} q_y)}. \tag{7}$$

Due to momentum conservation, electrons propagating through a k–q interface will conserve their wavevector component parallel to the interface. Thus, taking this interface to be located along the $\hat{y}$ axis, we will have always $k_y = q_y$. The q-region eigenenergy, associated with the eigenstate (6) and the Hamiltonian (5), is

$$E = \pm\sqrt{(q_x^2 + k_y^2)(\hbar\, v_F)^2 + t'^2}. \tag{8}$$

It is amusing to notice that the spectrum (8) has the same form as for the electrons in a graphene bilayer, when the two graphene planes are at different electrostatic potentials [36, 37]. Using equations (8) and (4), we write

$$v_F \hbar q_x = \sqrt{E^2 \cos^2(\theta) - t'^2} \tag{9}$$

and, depending on $E^2 \cos^2(\theta)$ being larger or smaller than t'^2, q_x may take a real or a pure imaginary value. Wave propagation follows for the former case, evanescent waves in the latter.

For a real q_x, and since $q_y = k_y$, we have

$$\sqrt{E^2 - t'^2}\sin(\phi) = |E|\sin(\theta) \tag{10}$$

where ϕ is the angle of propagation of the electron in the q-region (see figure 1). Equation (10) is just the usual Snell's law for electrons being refracted at the interface separating the k- and q-regions. We see that $\phi \geqslant \theta$ whenever $|E| > t'$.

2.1. Forward and backward propagation

We consider now the simple reflection in the interface, with the incident and the reflected waves both on the k- or on the q-region.

In the k-region, the $\hat{x}$ component of the wavevector of the reflected wave is symmetrical with respect to the incident wave. Thus, for this case, we have the following transformations under a reflection (see also figure 1):

$$k_x \to -k_x \qquad \text{and} \qquad \mathrm{e}^{\mathrm{i}\theta} \to \mathrm{e}^{\mathrm{i}(\pi-\theta)} = -\mathrm{e}^{-\mathrm{i}\theta}. \tag{11}$$

This leads to the generalization of equations (2) and (3):

$$u_\pm = \pm s\, \mathrm{e}^{\pm \mathrm{i}\theta}, \tag{12}$$

$$\psi_{\mathbf{k}}^{\pm} = \frac{1}{\sqrt{2}} \begin{pmatrix} 1 \\ u_\pm \end{pmatrix} \mathrm{e}^{\pm \mathrm{i} k_x x + \mathrm{i} k_y y}. \tag{13}$$

where the plus and minus signs refers to waves propagating, respectively, in the positive and negative directions of the $\hat{x}$ axis.

A similar reasoning leads to the generalization of (7) to $v(\mathbf{q}, s)$:

$$v_\pm = \frac{E - t'}{\hbar v_F (\pm q_x - \mathrm{i} k_y)}. \tag{14}$$

and, also, of the q-region wavefunction to

$$\psi_{\mathbf{q}}^{\pm} = \frac{1}{\sqrt{2}} \begin{pmatrix} 1 \\ v_\pm \end{pmatrix} \mathrm{e}^{\pm \mathrm{i} q_x x + \mathrm{i} k_y y}. \tag{15}$$

The differences we have just highlighted in the wavefunctions and coefficients for forward and backward propagating particles can be also seen in the differences in positive and negative angles of incidence in the interface. These changes are useful when a guiding-wave kind of device is made. Let us therefore analyze the case when $k_y \to -k_y$. If in equation (11) we keep k_x unaltered and 'reflect' instead k_y we would obtain

$$k_y \to -k_y \qquad \text{and} \qquad \mathrm{e}^{\mathrm{i}\theta} \to \mathrm{e}^{-\mathrm{i}\theta}, \tag{16}$$

with similar relations for ϕ, the angle in the q-region. For this case, we get

$$v_\pm(-\phi) = -v_\mp(\phi) \qquad \text{and} \qquad u_\pm(-\theta) = -u_\mp(\theta). \tag{17}$$

Apart from a minus sign, these relations shows that the operation of changing the sign of k_y (i.e. the angle of incidence) is equivalent to the one of changing the sign of k_x (q_x in the q-region). Of course, the extra minus sign on the right-hand side of both expressions in equation (17) is of no consequence within the calculation of reflection and transmission coefficients that follows.

2.2. Real and evanescent waves in the q-region

Since in the q-region there is a gap in the energy spectrum then q_x can take both real and pure imaginary values. In the first case, we have wave propagation in this region, in the latter just evanescent waves. No simple expression as the one given by equation (12) can be written in this case. Instead, we need to consider separately the cases where q_x is a real or a pure imaginary number.

2.2.1. For q_x real. For real q_x, we can write a similar expression to the one in equation (12):

$$v_\pm = \pm v \mathrm{e}^{\pm \mathrm{i}\phi}, \tag{18}$$

with ϕ given by equation (10) and

$$v = \frac{E - t'}{v_F \hbar |q|} = \frac{E - t'}{\sqrt{E^2 - t'^2}}, \tag{19}$$

where equation (8) was used.

2.2.2. For q_x pure imaginary. Since k_y is always a real number, equation (14) implies that, if q_x is a pure imaginary, $v_\pm$ is also, and then

$$v_\pm = \mp \mathrm{i} \nu_\pm, \tag{20}$$

where

$$\nu_\pm = \pm \frac{E - t'}{\hbar v_F (\pm k_y - \alpha)}, \tag{21}$$

with the real *absorption coefficient* α defined as $q_x = \mathrm{i}\alpha$, and α given by

$$\alpha = (v_F \hbar)^{-1} \sqrt{t'^2 - E^2 \cos(\theta)^2}. \tag{22}$$

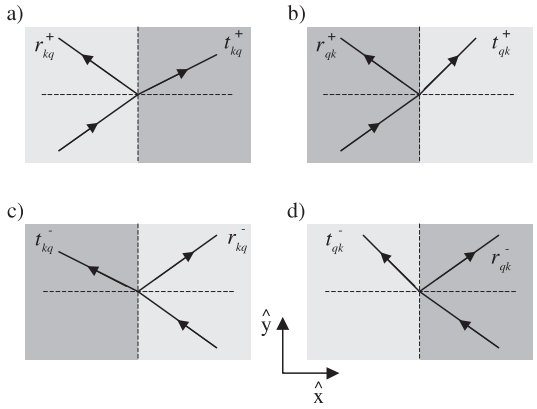

Figure 2. The four different possible cases for reflection/transmission in an interface between k and q regions.

2.2.3. Complex conjugate of the $u_\pm$ and $v_\pm$ coefficients. For the calculation of the intensity reflection and transmission coefficient we will need to deal with the complex conjugate of the $u_\pm$ and $v_\pm$ coefficients. The definition (12) for $u_\pm$ implies that

$$u_\pm^* = -u_\mp. \tag{23}$$

In the case of $v_\pm$, its complex conjugate depends on the fact of having a real or imaginary q_x:

$$v_\pm^* = \begin{cases} -v_\mp & \text{if } q_x \text{ is real} \\ -v_\pm & \text{if } q_x \text{ is imaginary.} \end{cases} \tag{24}$$

3. Transmission and reflection at the interface: the step case

3.1. Reflection and transmission amplitude coefficients

We compute now the reflection and transmission amplitude coefficients for electrons crossing an interface between a k- and a q-region. Unlike what happens in optics, and due to the differences in back and forward propagation, we will need to consider not only two but four different cases: electrons crossing the interface coming from the k-region in the forward and backward senses, and those crossing the interface coming from the q-region, also propagating in the positive and negative senses of the x axis. These four cases are summarized in figure 2.

3.1.1. Propagation from a k- into a q-region. We start by deriving the amplitude reflection and transmission coefficients, which will be denoted as $r_{kq}^\pm$ and $t_{kq}^\pm$, respectively, for the case of the propagation from a k- into a q-region. This situation is described in figure 1 and also in figure 2(a).

Since there is a partially reflected wave, the total wavefunction in the k-region must be written as an superposition of one associated with the incident electrons and the other with those that are reflected:

$$\Psi_k(\mathbf{r}) = A\,\psi_{\mathbf{k}}^+ + B\,\psi_{\mathbf{k}}^-. \tag{25}$$

A and B are the normalized amplitudes for the incident and reflected wavefunctions. In the q-region, with C the amplitude of the transmitted wavefunction, we have

$$\Psi_q(\mathbf{r}) = C\,\psi_{\mathbf{q}}^+. \tag{26}$$

Using equations (25) and (26), and imposing the continuity condition of the particle's wavefunction at the interface, i.e. $\Psi_k(x, y = 0) = \Psi_q(x, y = 0)$, we find

$$r_{kq}^+ = \frac{B}{A} = \frac{v_+ - u_+}{u_- - v_+} \qquad \text{and} \qquad t_{kq}^+ = \frac{C}{A} = 1 + r_{kq}^+, \tag{27}$$

where the superscript $+$ recalls that the incident wavefunction is, in this case, traveling in the positive direction of the x axis.

Had we considered the case where the particles travel in the backward direction, represented by figure 2(c), we would have obtained

$$r_{kq}^- = \frac{v_- - u_-}{u_+ - v_-} \qquad \text{and} \qquad t_{kq}^- = 1 + r_{kq}^-. \tag{28}$$

This result can be obtained simply by exchanging the plus by the minus signs in equation (27).

3.1.2. Propagation from the q- into the k-region. For computing the reflection and transmission coefficients for the cases where the electrons come from the q-region into the k-region, $r_{qk}^\pm$ and $t_{qk}^\pm$, we need only to exchange $u \leftrightarrow v$ in the corresponding backward and forward expressions (27) and (28). The result is

$$r_{qk}^\pm = \frac{u_\pm - v_\pm}{v_\mp - u_\pm} \qquad \text{and} \qquad t_{qk}^\pm = 1 + r_{qk}^\pm. \tag{29}$$

3.2. Amplitude coefficients: general algebraic relations.

It will be very useful in the following, for expression simplification purposes, to derive the simple relations between the reflection and transmission amplitude coefficients. Similar relations to those we present here exist also for the photons' optics case. For instance, we may write $\pm r_{12} + t_{12} = 1$ when a light beam is reflected and refracted in a diopter between regions 1 and 2, with the plus or minus sign corresponding, respectively, to the cases where n_1, the index of refraction of medium 1, is smaller or larger than the one of region 2.

Here, however, we have that in general $r_{mn}^+ \neq r_{mn}^-$ (and similarly for the transmission coefficients) and these relations are less trivial (we have used the notation $m \neq n = \{k, q\}$).

Using the definitions in equations (27)–(29), we can write

$$\mathcal{R} + \mathcal{T} = 1, \tag{30}$$

where

$$\mathcal{R} = r_{kq}^+ r_{kq}^- = r_{qk}^+ r_{qk}^- \qquad \mathcal{T} = t_{qk}^+ t_{kq}^+ = t_{qk}^- t_{kq}^-. \tag{31}$$

These relations are general and do not depend on the q_x being real or imaginary. Another general relation, useful to simplify expressions of the transmission of multi-layered structures, is

$$r_{mn}^\pm r_{nm}^\mp = -\mathcal{R} \times \frac{t_{nm}^\mp}{t_{nm}^\pm}. \tag{32}$$

3.3. Intensity reflection and transmission coefficients

The general definitions for the intensity reflection and transmission coefficients are

$$\begin{aligned} R^{\pm}_{mn} &= r^{\pm}_{mn}\left(r^{\pm}_{mn}\right)^{*} \\ T^{\pm}_{mn} &= t^{\pm}_{mn}\left(t^{\pm}_{mn}\right)^{*} = 1 - R^{\pm}_{mn}, \end{aligned} \tag{33}$$

where we keep the same notation as before. We will consider now, separately, the cases where q_x is a real number or a pure imaginary.

3.3.1. For q_x real. For q_x a real number, we note first that for any $m \neq n = \{k, q\}$

$$\begin{aligned} \left(r^{\pm}_{mn}\right)^{*} &= r^{\mp}_{mn} \\ \mathcal{R} &= \mathcal{R}^{*}. \end{aligned} \tag{34}$$

These relations are just a consequence of the definitions of $r^{\pm}_{mn}$ in equations (27)–(29) and in equations (23) and (24). Using equation (34) in equation (33) results in

$$R = \mathcal{R} \qquad \text{and} \qquad T = \mathcal{T} \quad \text{for } q_x \text{ real},$$

which is valid, for both interfaces and both directions of propagation. Furthermore, using equation (30) we get

$$R + T = 1,$$

an expected result.

Explicitly, the $\mathcal{R}$ coefficient defined in equation (31) is given by

$$\mathcal{R} = \frac{(v_+v_- - 1) - (u_-v_+ + u_+v_-)}{(v_+v_- - 1) - (u_-v_- + u_+v_+)}.$$

Making use of equations (14) and (12), we may write

$$v_+v_- = -v^2, \qquad u_{\pm}v_{\mp} = -s\,v\,\mathrm{e}^{\pm \mathrm{i}(\theta-\phi)} \qquad \text{and}$$

$$u_{\pm}v_{\pm} = s\,v\,\mathrm{e}^{\pm \mathrm{i}(\theta+\phi)},$$

where v is given by equation (7) and ϕ by equation (10). Using these expressions we obtain

$$\mathcal{R} = \frac{1 + v^2 - 2\,s\,v\cos(\theta - \phi)}{1 + v^2 + 2\,s\,v\cos(\theta + \phi)},$$

where

$$v\cos(\theta \pm \phi) = \frac{v_F\hbar}{E + t'}\left(q_x\cos(\theta) \mp k_y\sin(\theta)\right).$$

Finally, after algebraic simplification, we obtain

$$R = \mathcal{R} = \frac{k_x - q_x}{k_x + q_x}. \tag{35}$$

3.3.2. For q_x pure imaginary. For q_x a pure imaginary, we see that

$$\begin{aligned} \left(r^{\pm}_{mn}\right)^{*} r^{\pm}_{mn} &= 1 \\ \mathcal{R}\,\mathcal{R}^{*} &= 1. \end{aligned} \tag{36}$$

Using these relations along with equation (33), we straightforwardly obtain

$$R^{\pm}_{kq} = 1 \qquad \text{and} \qquad T^{\pm}_{kq} = 0 \qquad \text{with } q_x \text{ a pure imaginary.} \tag{37}$$

This is an expected result since the transmission $T = 1 - R$ must be zero in the case where the wave in the k-region enters in the gap of the q-region. If the incident wave propagates in the gap region, i.e. it is an evanescent wave, the coefficients $R^{\pm}_{qk}$ and $T^{\pm}_{qk}$ are physically meaningless.

We see from the second expression in (36) that $\mathcal{R}$ is a modulo 1 complex quantity. It may be written as

$$\mathcal{R} = \mathrm{e}^{\mathrm{i}2\varphi}, \tag{38}$$

with 2φ a convenient definition of its argument. To compute this angle, in the spirit of equation (22), we replace q_x by $\mathrm{i}\alpha$ in equation (35) to obtain

$$\mathcal{R} = \frac{k_x - \mathrm{i}\alpha}{k_x + \mathrm{i}\alpha}.$$

Computing the real part of this quantity, we get

$$\cos(2\varphi) = \frac{2E^2\cos(\theta)^2}{t'^2} - 1$$

and, after straightforward manipulation,

$$\cos(\varphi)\,t' = \cos(\theta)\,|E| \quad \text{or else} \quad \tan(\varphi) = \frac{\alpha}{k_x}, \tag{39}$$

a Snell type expression for the q_x pure imaginary case.

Since $R = \mathcal{R}\mathcal{R}^{*} = 1$ for q_x a pure imaginary, a general expression for the intensity reflection and transmission coefficients (valid for q_x both real and pure imaginary) is given by

$$\begin{aligned} R &= 1 - T \\ &= \left|\frac{k_x - q_x}{k_x + q_x}\right| \\ &= \left|\frac{1 + v^2 - 2s\,v\cos(\theta - \phi)}{1 + v^2 + 2s\,v\cos(\theta + \phi)}\right|. \end{aligned} \tag{40}$$

Naturally, equation (40) depends on t', since v, θ and ϕ depend on this quantity. When one considers the case $\theta = \phi = t' = 0$ one obtains $R = 0$. This expression is plotted in a density/contour plot in figure 3.

4. The barrier

With the above definitions, the computation of transmission and reflection coefficients for any type of multi-interface device follows similar expressions to those found in normal optics[1]. To illustrate this, we consider in the following a heterostructure made of a q-region of width w placed between two semi-infinite slabs of k-regions, as shown in figure 4. Our goal will be the derivation of the intensity transmission coefficient for this case, which we will denote by T_{b}. We notice that results for barriers of the same height when the spectrum of the electrons is linear in every spatial region was considered in [38].

[1] There is no analog, however, for the gap region with normal incidence.

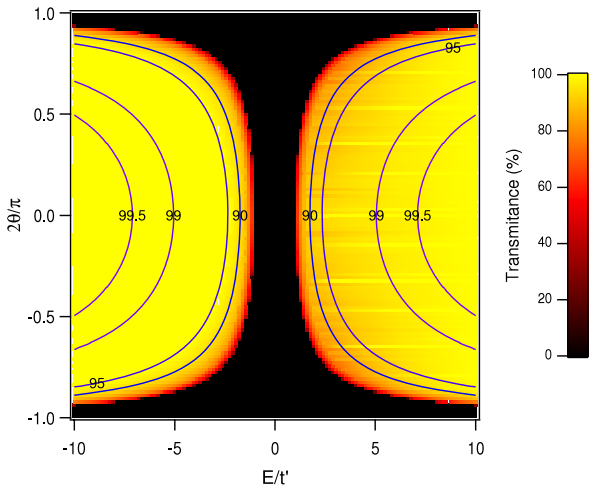

Figure 3. Intensity transmission for particles crossing the interface from a k-region into a q-region. The black region corresponds to a zero transmission, a case that corresponds to the total internal reflection in the usual photonic optics.

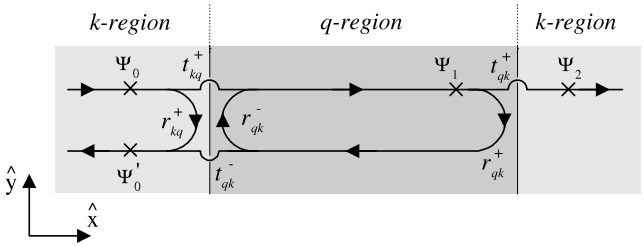

Figure 4. Barrier: scheme for the computation of the transmission.

In figure 4, the wavefunction Ψ_1 describes an electron, traveling in the positive direction of the $\hat{x}$ axis, just before crossing the *diopter* $q - k$. This wavefunction can be seen as resulting from the coherent superposition of two wavefunctions, one being itself after a round trip in the q-region, given by $\Psi_1\, t^+_{qk} t^-_{qk}\, \mathrm{e}^{\mathrm{i}2q_x w}$, and another one which is the *incident* wavefunction Ψ_0 after crossing the first interface $k-q$, equal to $\Psi_0\, t^+_{kq}\, \mathrm{e}^{\mathrm{i}q_x w}$. Adding these two contribution and solving in order to find Ψ_1 we obtain

$$\Psi_1 = \Psi_0 \frac{t^+_{kq}\, \mathrm{e}^{\mathrm{i}q_x w}}{1 - r^+_{qk} r^-_{qk}\, \mathrm{e}^{\mathrm{i}2q_x w}}.$$

If we denote the amplitude transmission coefficient for this barrier as $t_\mathrm{B} = \Psi_2/\Psi_0$ and using the fact that $\Psi_2 = t^+_{qk}\Psi_1$, we finally obtain

$$t_\mathrm{B} = \frac{\mathcal{T}\mathrm{e}^{\mathrm{i}q_x w}}{1 - \mathcal{R}\mathrm{e}^{\mathrm{i}2q_x w}} \tag{41}$$

where the definitions (30) were used.

4.1. q_x real: free propagation

If there is wave propagation in the q-region, q_x is real, $\mathcal{R} = R$ and $\mathcal{T} = T$, and

$$T_\mathrm{B} = t_\mathrm{B}\, t^*_\mathrm{B} = 1 - R_\mathrm{B}$$
$$= \left[1 + \left(\frac{2}{\pi}\mathcal{F}\right)^2 \sin^2(q_x w)\right]^{-1}. \tag{42}$$

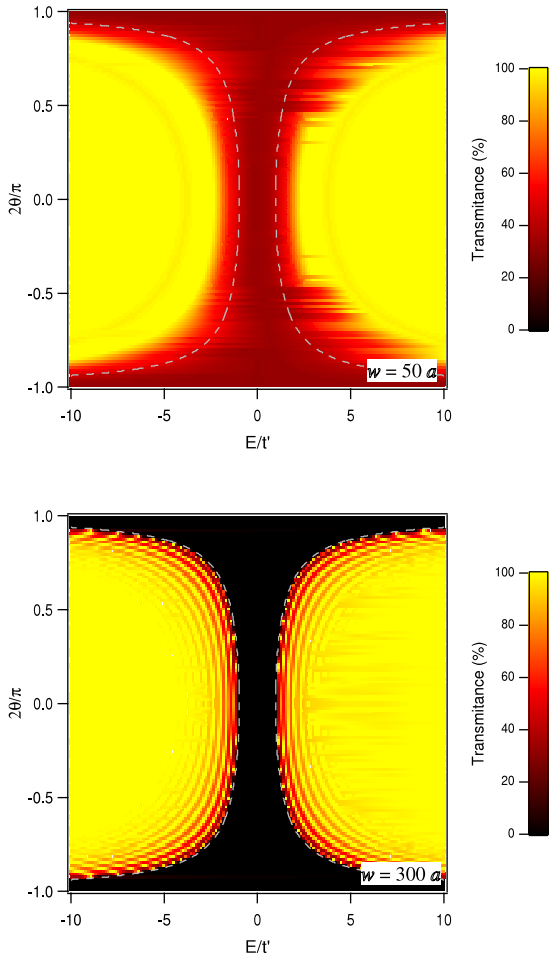

Figure 5. Transmission of a barrier for a q-region width of $w = 50a$ (top) and $w = 300a$ (bottom). For a sufficiently narrow width, the wave tunnels across the q-region resulting in a non-null transmission. In optics, this behavior is known as *frustrated* total internal reflection. The dashed lines mark the region where, in the step, the transmission is zero.

where we used the finesse definition

$$\mathcal{F} = \pi \frac{\sqrt{R}}{T} = \frac{\pi}{2}\frac{t'}{q_x}, \tag{43}$$

to highlight the similarity with an Fabry–Pérot solid etalon (made of glass, for example) in the usual optics [39]. However, this similarity is elusive. In the solid etalon case, in general, the finesse is almost a constant coefficient since the interfaces' reflectivities (e.g. in a glass–air diopter) has a small dependence on the energy (optical resonances are typically far from the visible part of the spectrum and there's no gap as in the case of the graphene with a mass term). In the case treated here, $\mathcal{F}$ has a strong dependence on the energy E of the particles and, furthermore, there is also a gap present. We will revisit a Fabry–Pérot type of device later in this work.

4.2. Inside the gap: frustrated total internal reflection

Inside the gap, q_x is pure imaginary and there's no wave propagation. This is similar to the total internal reflection in

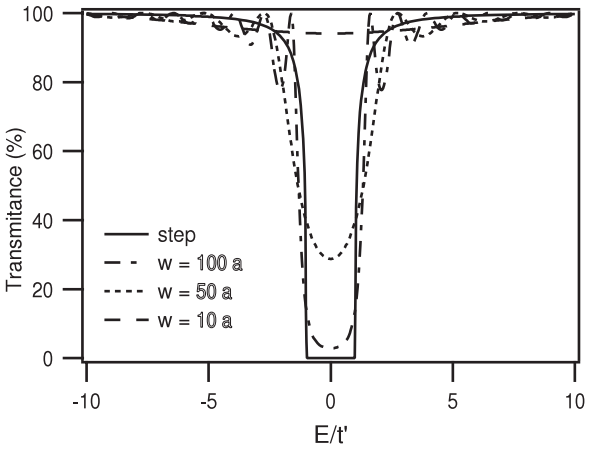

Figure 6. Transmission coefficient for a simple step and several barriers for normal incidence. In the barrier case, there is a *frustrated* total internal reflection and, in the gap, the transmission is non-zero and increases with decreasing values of the width of the q-region.

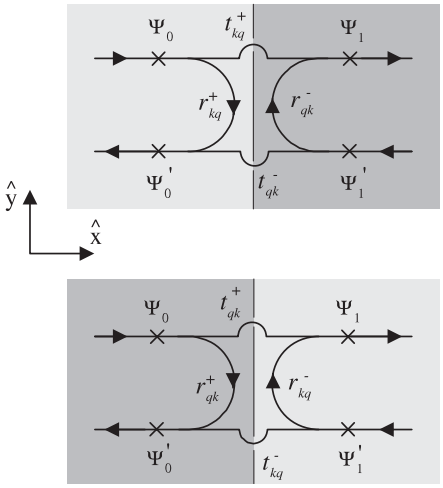

Figure 8. Schemes for the computation of the transfer matrices.

optics, where only an evanescent wave exists that carries no energy (since, in here, the coefficient $R_{kq} = 1$) and decays exponentially in the x direction (although keeping the phase term $e^{ik_y y}$ in the y direction).

However, by placing a k-region nearby the evanescent wave, some of the energy of the totally reflected wave tunnels throughout the gap region, a phenomena known in optics as *frustrated total internal reflection*. This phenomena is also described by equation (42), whenever q_x becomes pure imaginary. In this case, replacing $q_x = i\alpha$ and using the definitions (22) and (38) we may simplify equation (42) to

$$T_B = t_B t_B^* = 1 - R_B = \frac{1}{1+\zeta}, \tag{44}$$

where we have used the definition

$$\zeta = \frac{\sinh^2(\alpha w)}{\sin^2(\varphi)}, \tag{45}$$

which will be used in the following. Figure 5 shows the transmission for two barriers of different widths. Figure 6 shows the transmission at normal incidence; clearly when the energy is inside the gap the transmission is smaller than one and there is no Klein paradox. If $E = 0$, equation (39) implies that $\varphi = -\pi/2$ and $\alpha = t'/v_F\hbar$. T_B is, in this case, independent of θ and is equal to

$$T_B(E=0) = \cosh^{-2}\left(w\frac{t'}{v_F\hbar}\right). \tag{46}$$

This behavior is clearly shown in the left panel of figure 7. In the right panel of figure 7 it is shown how this tunneling transmittance at zero energy varies with the barrier width. A 50% reduction is accomplished for a barrier with a width of approximately 36 a.

5. Transfer matrices

The method used in section 8 for computing t_B, although being simple, becomes very difficult to handle for more complex heterostructures with more than two interfaces. These types of cases are usually treated with the use of *transfer* matrices. These will be computed in the following. Figure 8 shows the

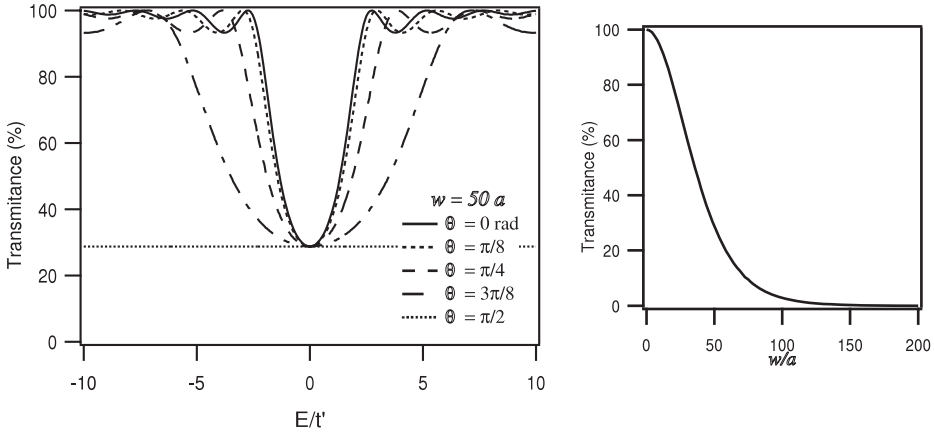

Figure 7. Left: transmission coefficient for a barrier with a width $50a$ and for different angles of incidence θ. At $E = 0$, all curves have the same value and, for $\theta = \pi/2$, the transmission is a delta function at $E = 0$. Right: zero energy transmission coefficient of a barrier as a function of its width w.

scheme used to compute the transfer matrix in an interface $k-q$ and $q-k$. In both cases, our goal is to derive Ψ_1 and Ψ_1' from the knowledge of Ψ_0 and Ψ_0'. Defining

$$\begin{pmatrix} \Psi_1 \\ \Psi_1' \end{pmatrix} = \mathbf{M}_{mn} \begin{pmatrix} \Psi_0 \\ \Psi_0' \end{pmatrix},$$

where $\mathbf{M}_{mn}$ is the transfer matrix for the generic $m-n$ interface, and using equation (31), we obtain the result

$$\mathbf{M}_{mn} = \begin{bmatrix} \frac{1}{t_{nm}^{+}} & \frac{r_{nm}^{-}}{t_{nm}^{-}} \\ -\frac{r_{mn}^{+}}{t_{nm}^{-}} & \frac{1}{t_{nm}^{-}} \end{bmatrix}. \tag{47}$$

The determinant of this matrix is given by

$$\mathrm{Det}(\mathbf{M}_{kq}) = \left[\mathrm{Det}(\mathbf{M}_{qk})\right]^{-1} = \frac{t_{kq}^{+}}{t_{qk}^{-}}. \tag{48}$$

As expected, $\mathrm{Det}(\mathbf{M}_{kq} \times \mathbf{M}_{qk}) = 1$. The free propagation of a particle in a k- and in a q-region of width ξ is given, respectively, by

$$\mathbf{L}_k(\xi) = \begin{bmatrix} \mathrm{e}^{\mathrm{i}k_x\xi} & 0 \\ 0 & \mathrm{e}^{-\mathrm{i}k_x\xi} \end{bmatrix}; \qquad \mathbf{L}_q(\xi) = \begin{bmatrix} \mathrm{e}^{\mathrm{i}q_x\xi} & 0 \\ 0 & \mathrm{e}^{-\mathrm{i}q_x\xi} \end{bmatrix}. \tag{49}$$

6. The diode

We consider now a more complex system composed by a sandwich of two q-regions of width w separated by a slab of a k-region with width d, inside two semi-infinite k-regions. The geometry of the system is represented in figure 9. To derive the amplitude transmission coefficient of such a structure we need to compute the expression

$$t_d = \mathbf{M}_{qk}\,\mathbf{L}_q(w)\,\mathbf{M}_{kq}\,\mathbf{L}_k(d)\,\mathbf{M}_{qk}\,\mathbf{L}_q(w)\mathbf{M}_{kq}.$$

The result of this expression can be simplified using equation (32), resulting in

$$t_{\mathrm{D}} = \frac{\mathcal{T}^2\,\mathrm{e}^{2\mathrm{i}q_x w}}{(\mathcal{R}\,\mathrm{e}^{2\mathrm{i}q_x w}-1)^2 - \mathcal{R}(\mathrm{e}^{2\mathrm{i}q_x w}-1)^2\,\mathrm{e}^{2\mathrm{i}k_x d}}.$$

For the most important case where the q-regions are barriers with energy higher than the energy of the particles, we have a resonant diode. In this case and using the definitions (22) and (38) we get

$$t_{\mathrm{D}} = t_{\mathrm{B}}^2 \times \left[1 - \frac{\sinh^2(\alpha w)}{\sinh^2(\alpha w + \mathrm{i}\varphi)}\,\mathrm{e}^{\mathrm{i}2k_x d}\right]^{-1}, \tag{50}$$

where t_{B} is the amplitude transmission for a simple barrier, given by equation (41).

We may simplify equation (50) by expanding the term $\sinh(\alpha w + \mathrm{i}\varphi)$ and expressing the result in a complex polar representation. Doing this and using the definition for ζ in equation (45) we obtain

$$\frac{\sinh^2(\alpha w)}{\sinh^2(\alpha w + \mathrm{i}\varphi)} = \frac{\zeta}{1+\zeta}\exp(\mathrm{i}2\widetilde{\varphi})$$

with the phase term argument given by

$$\widetilde{\varphi} = -\arctan[\coth(\alpha w)\tan(\varphi)].$$

The intensity transmission coefficient can now be easily computed, being equal to

$$T_{\mathrm{D}} = \frac{1}{1 + \left(\frac{2}{\pi}\mathcal{F}_{\mathrm{D}}\right)^2 \sin^2(\widetilde{\varphi} + k_x d)}, \tag{51}$$

where now the *diode finesse* $\mathcal{F}_{\mathrm{D}}$ is given by

$$\mathcal{F}_{\mathrm{D}} = \pi\sqrt{\zeta(1+\zeta)}. \tag{52}$$

The transmission is represented in figure 10.

6.1. Revisiting the Fabry–Pérot: etalon made with 'mirrors'

The expression (51) results in the simple case of a Fabry–Pérot etalon if:

(i) $\alpha w \gg 1$, which implies $\coth(\alpha w) \cong 1$ and $\tilde{\varphi} \cong \varphi$;
(ii) $E \ll t'$, which implies that $\varphi \approx \pi/2$.

With these approximations we get

$$\mathcal{F}_{\mathrm{D}} = \frac{\pi}{2}\sinh(2\alpha w)$$

and then

$$T_{\mathrm{D}} = \frac{1}{1 + \sinh^2(2\alpha w)\cos^2(k_x d)}, \tag{53}$$

an expression that can be derived from a delta function potential treatment, treated in section 7.

6.2. The diode tunneling conductance

Let us now compute the tunneling conductance of the device as a function of the potential bias V, the chemical potential of the leads and the length w of the barrier. We shall assume that the device is operating in the region where the chemical potential of the leads lies inside the gap of the barrier. The total tunneling current density (i.e. the current per unit of cross-sectional length) through the device is given by

$$J(V,w) = -\frac{2e}{4\pi^2 v_F \hbar^2}\int \mathrm{d}\theta\, E\mathrm{d}E\,\cos\theta\, T(E,\theta) \times [f(E-\mu_L) - f(E-\mu_R)] \tag{54}$$

where $f(x) = (1+\mathrm{e}^{x/(k_{\mathrm{B}}T)})^{-1}$, $\mu_L = \mu + eV/2$, $\mu_R = \mu - eV/2$ and μ is the chemical potential of leads in the equilibrium state. The linear response conductance per unit of cross-sectional length is given, at zero temperature, by

$$G(\mu,w) = \frac{e^2}{\hbar}\frac{|\mu|}{3\pi^2 at}\int_{-\pi/2}^{\pi/2}\mathrm{d}\theta\,\cos\theta\, T(\mu,\theta). \tag{55}$$

In figure 11 we plot $G(\mu,w)$ as a function of μ for several widths w. It is clear that the value of $G(\mu,w)$ may change by several orders of magnitude, close to $\mu = 0$ by a small change of μ. Naturally for wider barriers one obtains a smaller conductance.

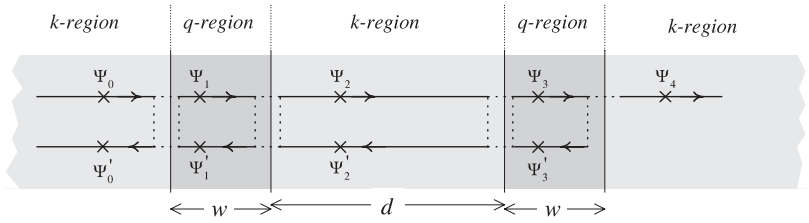

Figure 9. The diode heterostructure: two thin slabs of q-regions of width w separated by a k-region of width d, all inside semi-infinite slabs of k-regions.

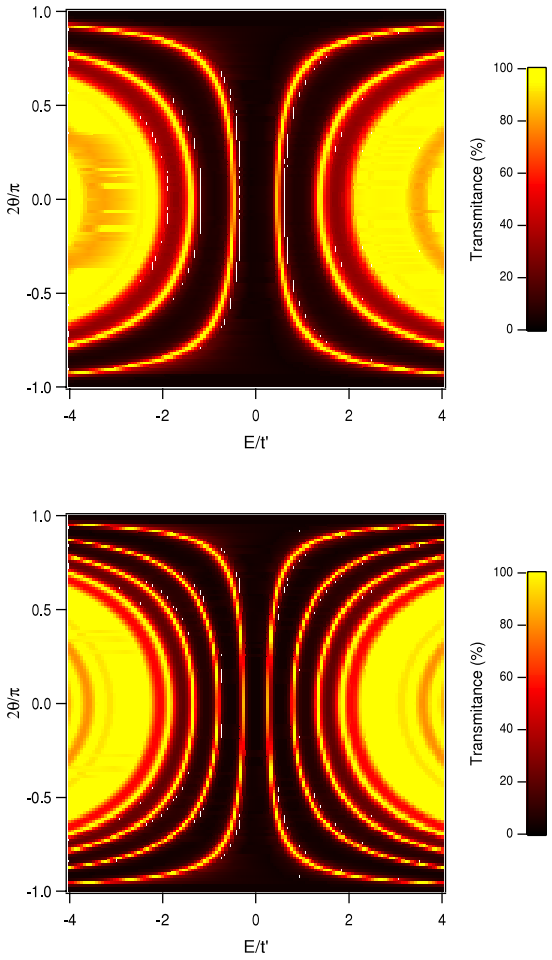

Figure 10. Transmission of a diode structure with $w = 50a$ and $d = 100a$ (top) and $d = 200a$ (bottom).

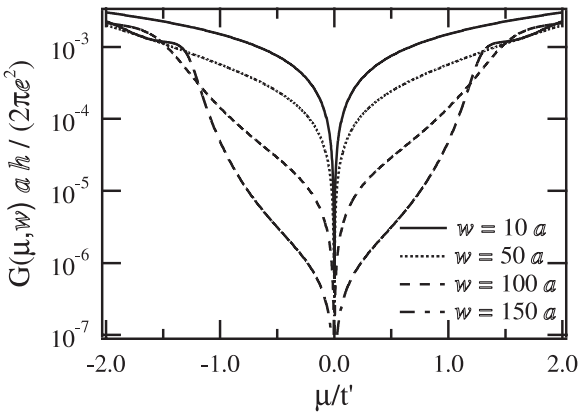

Figure 11. Linear response conductance $G(\mu, w)$, per Dirac cone, as a function of the chemical potential μ, for different values of the width w. The hopping matrix t is taken to be $t = 2.7$ eV and $t' = 0.1$ eV.

6.3. A limiting case

The limiting case of a barrier can be represented by a delta function potential, $V(x, y) = g\sigma_z\delta(x)$. (See the next section for a complete discussion of delta function potentials in the Dirac equation.) It is interesting to compute the reflected flux for both Schrödinger and Dirac electrons for this potential. In the first case one obtains

$$R = \frac{(2mg/\hbar^2)^2}{4k_F^2\cos^2\theta + (2mg/\hbar^2)^2}, \tag{56}$$

whereas for Dirac electrons the result is

$$R = \tanh^2[g/(\hbar v_F)]\,. \tag{57}$$

It is clear that, for electrons in graphene, R is angular and energy-independent. For the case $g \gg \hbar v_F$ the reflection tends to unity.

7. The diode: a limiting case

Finally we want to discuss a limiting case of the resonant tunneling diode made of graphene. The device is represented in figure 9. The corresponding study for Schrödinger electrons was done by Tsu and Esaki [41].

A limiting situation of the device described in figure 9 is one where the barriers are described by a scalar Lorentz potential of the form

$$\begin{aligned} V(x, y) &= \lim_{\epsilon\to 0} g\frac{1}{2\epsilon}[1 - \theta(|x| - \epsilon)]\sigma_z \\ &\quad + \lim_{\epsilon\to 0} g\frac{1}{2\epsilon}[1 - \theta(|x - d| - \epsilon)]\sigma_z \\ &= g\sigma_z[\delta(x) + \delta(x - d)]. \end{aligned} \tag{58}$$

The connection with the true barrier is made by identifying g with $\alpha t' wa$, with α a numerical constant of dimensions the inverse of length. This form of the potential is equivalent to a mass term and therefore to a gap in the spectrum. However, given the short range nature of the potential, its effect comes

only in the boundary conditions imposed on the wavefunction at the potential position.

The problem of Dirac electrons in delta function potentials has been studied in the past [42, 43] and is not without subtleties [44–46]. The subtleties can be traced back to the problem of evaluating the integral

$$\int_{-\epsilon}^{\epsilon} f(x)\delta(x)\,\mathrm{d}x, \tag{59}$$

where $f(x)$ is a discontinuous function at $x = 0$. If we try to solve the problem of Dirac electrons with a delta function potential using the same trick [40] one uses for Schrödinger electrons we face the problem defined by the integral (59). This is so because the wavefunction of Dirac electrons in a delta function potential is discontinuous at the point where the delta function is located. There are several strategies to overcome this difficulty [42–46]. The most straightforward was devised by McKellar and Stephenson [42, 43] and generalized by Dominguez-Adame and Maciá [45]. In short, the Dirac equation along the x direction can be written as

$$\frac{\mathrm{d}\phi(x)}{\mathrm{d}x} = \hat{G}(x)\phi(x), \tag{60}$$

where $\phi(x)$ is a spinor wavefunction. This problem can be formally solved as

$$\phi(x) = T_x \mathrm{e}^{\int_{x_0}^{x} \hat{G}(x)\,\mathrm{d}x}\phi(x_0), \tag{61}$$

where the operator T_x is the position order operator such that

$$T_x[\hat{G}(x)\hat{G}(y)] = \hat{G}(x)\hat{G}(y)\theta(x-y) + \hat{G}(y)\hat{G}(x)\theta(y-x). \tag{62}$$

Since we are interested in determining the boundary conditions obeyed by the wavefunction $\phi(x)$ at the delta function position we consider the infinitesimal interval $x \in [-\epsilon, \epsilon]$, obtaining

$$\phi(\epsilon) = T_x \mathrm{e}^{\int_{-\epsilon}^{\epsilon} \hat{G}(x)\,\mathrm{d}x}\phi(-\epsilon). \tag{63}$$

The integral is dominated by the delta function and for the problem we are treating in this paper we obtain the following boundary condition:

$$\phi(\epsilon) = \mathrm{e}^{-\mathrm{i}\frac{g}{v_F\hbar}\sigma_x\sigma_z}\phi(-\epsilon)\,. \tag{64}$$

To evaluate how the exponential acts on $\phi(-\epsilon)$ we use the Lagrange–Silvester formula [45] for a function $f(\boldsymbol{M})$ of a matrix $\boldsymbol{M}$:

$$f(\boldsymbol{M}) = f(\lambda_1)\frac{\mathbf{1}\lambda_2 - \boldsymbol{M}}{\lambda_2 - \lambda_1} + f(\lambda_2)\frac{\mathbf{1}\lambda_1 - \boldsymbol{M}}{\lambda_1 - \lambda_2}, \tag{65}$$

where $\lambda_{1,2}$ are the eigenvalues of $\boldsymbol{M}$. For the problem at hand, equation (65) leads to the following boundary condition around $x = 0$:

$$\begin{pmatrix}\phi_a(0^+)\\ \phi_b(0^+)\end{pmatrix} = \cosh\tilde{g}\begin{pmatrix}\phi_a(0^-)\\ \phi_b(0^-)\end{pmatrix} + \mathrm{i}\sinh\tilde{g}\begin{pmatrix}\phi_b(0^-)\\ -\phi_a(0^-)\end{pmatrix}. \tag{66}$$

where $\tilde{g} = \frac{g}{v_F\hbar}$ is an adimensional interaction constant and $0^{\pm}$ represent positive and negative infinitesimals. A similar boundary condition holds for $x = d$. For the potential (58) we can now define three different regions I, II and III, defined as $x < 0$, $0 < x < d$ and $x > d$, respectively. In each of these regions the wavefunction is a sum of two plane waves of opposite momentum along the x direction, with each plane wave multiplied by the coefficients A_Γ and B_Γ, where Γ = I, II and III label the three regions defined above.

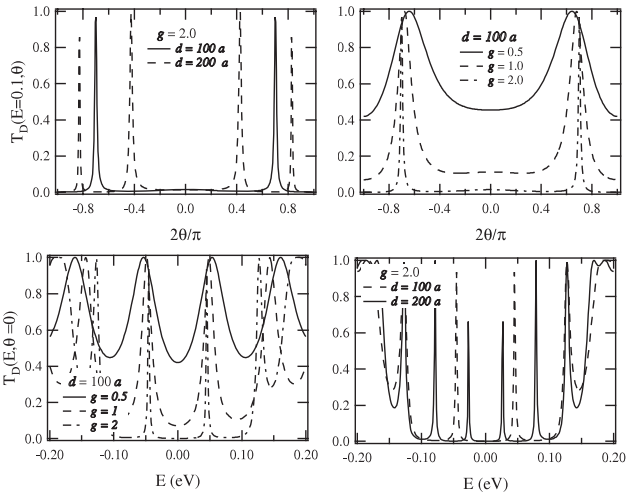

Figure 12. Top panels: transmitted flux $T_\mathrm{f}(E = 0.1, \theta)$ for fixed $\tilde{g} = 2$ and two $d = 100a, 200a$ and for fixed $d = 100a$ and three $\tilde{g} = 0.5, 1, 2$. Bottom panels: transmitted flux $T_\mathrm{f}(E, \theta = 0)$ for the same cases.

Once the matrix T has been computed (see the appendix) the reflection coefficient is obtained from

$$r = -\frac{T_{12}^*}{T_{11}^*}, \tag{67}$$

and the transmitted flux T_f from

$$T_\mathrm{f} = 1 - rr^*. \tag{68}$$

For the case of zero electrostatic potentials, $U_i = 0$, we obtain

$$T_\mathrm{f} = \frac{1}{1 + \sinh^2(2\tilde{g})\cos^2(2dk)}, \tag{69}$$

which is a similar expression to the one in (53) if $\tilde{g} = \alpha w$. It is simple to identify the limit $T \to 1$, which occurs when $2kd = (2n+1)\pi$, with $n = 0, 1, 2, \ldots$.

In figure 12 we show the transmitted flux $T_\mathrm{f}(E, \theta)$ as a function of the energy and of the angle θ. The barrier between the leads and the center of the device is represented by a delta function potential; therefore wider barriers are represented by larger values of $\tilde{g}$. From figure 12 we can see that, for larger values of $\tilde{g}$, the transmission in the forward direction is essentially zero except at some resonant energies, where the transmission goes to one. As a function of the angle we see that there are some angles for which the transmission is also one. When the length of the central part of the device is increased (larger d) the resonances become closer to each other and more resonances appear.

In figure 13 we present an intensity plot of $T_\mathrm{f}(E, \theta)$ for a device with $\tilde{g} = 0.5$ and $d = 200a$. In this figure we

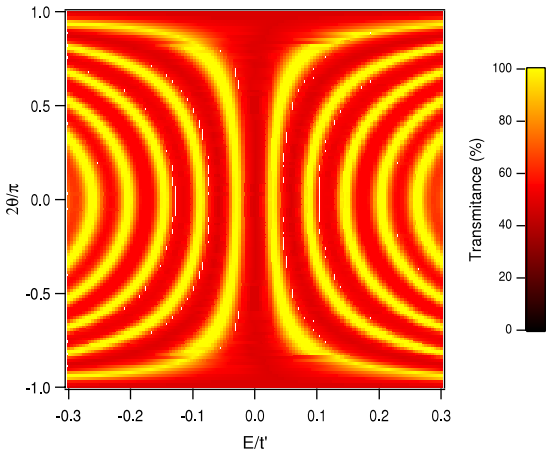

Figure 13. Intensity plot of $T_f(E, \theta)$ for a device with $\tilde{g} = 0.5$ and $d = 200a$. There are clearly well-defined regions of large intensity transmission.

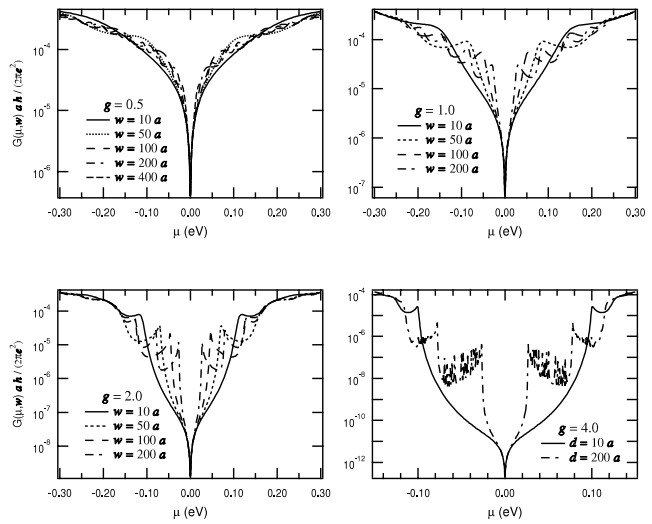

Figure 14. Linear response conductance per unit of cross-sectional length at zero temperature. The top panels show $G(\mu, d)$ with $\tilde{g} = 0.5, 1$ and the lower panels show the same quantity but for $\tilde{g} = 2, 4$.

can follow the evolution of the resonances in the E versus θ plane. The six lines of larger transmission are associated with the resonances we see in figure 12 for $\tilde{g} = 2$ and $d = 100a$.

As before, the linear response conductance per unit of cross-sectional length is given, at zero temperature, by equation (55) and represented in figure 14. For small values of $\tilde{g}$ the conductance shows smooth oscillations whereas for larger $\tilde{g}$ values strong resonances are observed. The number of observed resonances depends on the length d.

8. Final remarks

In this paper we discussed the tunneling properties of Dirac electrons in two dimensions when they traverse regions of space where the spectrum presents a finite energy gap. In the case we considered here, the gap is induced by depositing graphene on top of boron nitride, rendering, in this way, the sub-lattices A and B non-equivalent. The consequence is the opening of a gap in the energy spectrum that we have parameterized by the parameter $t' = 0.1t$. We have shown that the existence of an energy gap prevents the Klein paradox from taking place, a necessary condition for building nanoelectronic devices made of graphene. We have also shown that basic devices like a resonant tunneling diode can be made of graphene, by intercalating two regions where the spectrum of graphene presents a gap. We have also shown that simple analytical expressions can be derived for the tunneling through these types of heterostructures. In addition, we have shown that a limiting case of the resonant tunneling diode can be understood by using Dirac delta function potentials.

Clearly that one is led to think that a full description of the ballistic (no impurities) transport process in the system should also include the effect of temperature and phonons. We note, however, that the electron–phonon interaction has been shown to have a small effect in the optical conductivity of graphene [47]. Which means that phonons should not be very important in the description of the transport process. Also the polaronic effect leads to a renormalization of the velocity v_F in the k-region and to the renormalization of the effective mass $mv_F^2 = t'$ in the q-region. But since these two parameters can be considered as effective ones there is no point in including the polaronic effect explicitly. Concerning the temperature, clearly it will be of no importance when the chemical potential is above the gap. When the energy is in the gap there will certainly be temperature-activated transport adding on top of the tunneling current. For small temperatures this will be a small effect.

We believe our results of relevance for future nanoelectronics applications of graphene.

Acknowledgment

NMRP acknowledges the financial support from POCI 2010 via project PTDC/FIS/64404/2006.

Appendix. Details of section 7 results

We now give the details that allow one to derive the result (69). Applying boundary conditions derived in section 7 and a T-matrix description [40] for the scattering problem we obtain

$$\begin{pmatrix} A_{\rm III} \\ B_{\rm III} \end{pmatrix} = T \begin{pmatrix} A_{\rm I} \\ B_{\rm I} \end{pmatrix} = \begin{pmatrix} T_{11} & T_{12} \\ T_{12}^* & T_{11}^* \end{pmatrix} \begin{pmatrix} A_{\rm I} \\ B_{\rm I} \end{pmatrix} \tag{A.1}$$

with

$$T = V_3^{-1} M_2 V_2^{-1} M_1. \tag{A.2}$$

The several matrices involved in equation (A.2) are defined as

$$M_1 = \cosh \tilde{g} \begin{pmatrix} 1 & 1 \\ s_1 e^{i\theta_1} & -s_1 e^{-i\theta_1} \end{pmatrix} + i \sinh \tilde{g} \begin{pmatrix} s_1 e^{i\theta_1} & -s_1 e^{-i\theta_1} \\ -1 & -1 \end{pmatrix}. \tag{A.3}$$

$$V_2^{-1} = \frac{1}{2\cos\theta_2} \begin{pmatrix} e^{-i\theta_2} & s_2 \\ e^{i\theta_2} & -s_2 \end{pmatrix}, \tag{A.4}$$

$$M_2 = \cosh\tilde{g}\begin{pmatrix} e^{ik_2 d} & e^{-ik_2 d} \\ s_2 e^{i(\theta_2+k_2 d)} & -s_2 e^{-i(\theta_2+k_2 d)} \end{pmatrix} + i\sinh\tilde{g}\begin{pmatrix} s_2 e^{i(\theta_2+k_2 d)} & -s_2 e^{-i(\theta_2+k_2 d)} \\ -e^{ik_2 d} & -e^{-ik_2 d} \end{pmatrix}, \quad (A.5)$$

and

$$V_3^{-1} = \frac{1}{2\cos\theta_3}\begin{pmatrix} e^{-i(\theta_3+k_3 d)} & s_3 e^{-ik_3 d} \\ e^{i(\theta_3+k_3 d)} & -s_3 e^{ik_3 d} \end{pmatrix}. \quad (A.6)$$

The momenta k_2 and k_3 are given by

$$k_i = \frac{1}{v_F\hbar}\sqrt{(E-U_i)^2 - (E-U_1)^2\sin^2\theta_1}, \quad (A.7)$$

with $i = 2, 3$. The angles θ_i are defined as

$$\theta_i = \arctan\frac{k_y}{k_i}, \quad (A.8)$$

with $k_y = |E-U_1|\sin\theta_1/(v_F\hbar)$. The s_i functions are given by $s_i = \mathrm{sign}(E-U_i)$, with $i = 1, 2, 3$. The potential energies U_i represent some electrostatic potential created in the corresponding region. Although an analytical expression for T can be produced by carrying out the four matrix multiplications, the resulting expression is too cumbersome to be given here. In the special case that all $U_i = 0$, the matrix elements of T have a simple form given by

$$T_{11} = \cosh^2\tilde{g} + e^{-2idk}\sinh^2\tilde{g}, \quad (A.9)$$

and

$$T_{12} = -sie^{-i\theta}(1+e^{-2ikd})\cosh\tilde{g}\sinh\tilde{g}, \quad (A.10)$$

with $s = \mathrm{sign}\,E$, $k = |E|\cos\theta/(v_F\hbar)$ and θ the incident angle in the barrier.

References

[1] Novoselov K S, Geim A K, Morozov S V, Jiang D, Zhang Y, Dubonos S V, Grigorieva I V and Firsov A A 2004 *Science* **306** 666

[2] Novoselov K S, Jiang D, Booth T, Khotkevich V V, Morozov S M and Geim A K 2005 *Proc. Natl Acad. Sci.* **102** 10451

[3] Novoselov K S, Geim A K, Morozov S V, Jiang D, Katsnelson M I, Grigorieva I V, Dubonos S V and Firsov A A 2005 *Nature* **438** 197

[4] Zhang Y, Tan Y-W, Stormer H L and Kim P 2005 *Nature* **438** 201

[5] Tan Y-W, Zhang Y, Bolotin K, Zhao Y, Adam S, Hwang E H, Das Sarma S, Stormer H L and Kim P 2007 *Preprint* 0705.1102

[6] Hong S N and Ando T 1998 *J. Phys. Soc. Japan* **67** 2421

[7] Ando T, Zheng Y and Suzuura H 2002 *J. Phys. Soc. Japan* **71** 1318

[8] Peres N M R, Guinea F and Castro Neto A H 2006 *Phys. Rev.* B **73** 125411

[9] Ziegler K 2007 *Phys. Rev.* B **75** 233407

[10] Tworzydlo J, Trauzettel B, Titov M, Rycerz A and Beenakker C W J 2006 *Phys. Rev. Lett.* **96** 246802

[11] Katsnelson M I, Novoselov K S and Geim A K 2006 *Nat. Phys.* **2** 620

[12] Bai C and Zhang X 2007 *Phys. Rev.* B **76** 75430

[13] Klein O 1929 *Z. Phys.* **53** 157

[14] Calogeracos A and Dombey N 1999 *Contemp. Phys.* **40** 313

[15] Itzykson C and Zuber J-B 1985 *Quantum Field Theory* (New York: McGraw-Hill) ch 2

[16] Cheianov V V and Fal'ko V I 2006 *Phys. Rev.* B **74** 041403

[17] Cheianov V V, Fal'ko V and Altshuler B L 2007 *Science* **315** 1252

[18] Son Y-W, Cohen M L and Louie S G 2006 *Phys. Rev. Lett.* **97** 216803

[19] Yan Q, Huang B, Yu J, Zheng F, Zang J, Wu J, Gu B-L, Liu F and Duan W 2007 *Nano Lett.* **6** 1469

[20] Castro E V, Peres N M R, Lopes dos Santos J M B, Castro Neto A H and Guinea F 2008 *Phys. Rev. Lett.* **100** 026802
Castro E V, Peres N M R and Lopes dos Santos J M B 2007 *Phys. Status Solidi* b **244** 2311
Castro E V, Peres N M R and Lopes dos Santos J M B 2008 *Preprint* 0801.2788

[21] Giovannetti G, Khomyakov P A, Brocks G, Kelly P J and van den Brink J 2007 *Phys. Rev.* B **76** 73103

[22] Lu Y H, He P M and Feng Y P 2007 *Preprint* 0712.4008

[23] Zupan J 1972 *Phys. Rev.* B **6** 2477

[24] Titov M and Beenakker C W J 2006 *Phys. Rev.* B **74** 041401

[25] Moghaddam A G and Zareyan M 2007 *Appl. Phys.* A **89** 579

[26] Robinson J P and Schomerus H 2007 *Phys. Rev.* B **76** 115430

[27] Jayasekera T and Mintmire J W 2007 *Nanotechnology* **18** 424033

[28] Wakabayashi K, Takane Y and Sigrist M 2007 *Phys. Rev. Lett.* **99** 36601

[29] Titov M 2007 *Europhys. Lett.* **79** 17004

[30] Geim A K and Novoselov K S 2007 *Nat. Mater.* **6** 183

[31] Castro Neto A H, Guinea F and Peres N M R 2006 *Phys. World* **19** (Nov.) 33

[32] Katsnelson M I 2007 *Mater. Today* **10** 20

[33] Geim A K and MacDonald A H 2007 *Phys. Today* **60** 35

[34] Castro Neto A H, Guinea F, Peres N M R, Novoselov K S and Geim A K 2007 *Preprint* 0709.1163

[35] Beenakker C W 2007 *Preprint* 0710.3848

[36] McCann E 2006 *Phys. Rev.* B **99** 216802

[37] Milton Pereira J Jr, Vasilopoulos P and Peeters F M 2007 *Nano Lett.* **7** 946

[38] Barbier M, Peeters F M, Vasilopoulos P and Milton Pereira J Jr 2008 *Phys. Rev.* B **77** 115446
Milton Pereira J Jr, Peeters F M and Vasilopoulos P 2007 *Appl. Phys. Lett.* **90** 132122

[39] Born M and Wolf E 1997 *Principles of Optics: Electromagnetic Theory of Propagation, Interference and Diffraction of Light* 6th edn (Cambridge: Cambridge University Press)

[40] Davies J H 1998 *The Physics of Low-Dimensional Semiconductors* (Cambridge: Cambridge University Press) ch 5

[41] Tsu R and Esaki L 1973 *Appl. Phys. Lett.* **22** 562

[42] Bruce H, McKellar J and Stephenson G J Jr 1987 *Phys. Rev.* A **36** 2566

[43] McKellar B H J and Stephenson G J Jr 1987 *Phys. Rev.* C **35** 2262

[44] Sutherland B and Mattis D C 1981 *Phys. Rev.* A **24** 1194

[45] Dominguez-Adame F and Maciá E 1989 *J. Phys. A: Math. Gen.* **22** L419

[46] Roy C L 1993 *Phys. Rev.* A **47** 3417

[47] Stauber T and Peres N M R 2008 *J. Phys.: Condens. Matter* **20** 055002